DOI: 10.1021/cg900785f

CRYSTAL GROWTH & DESIGN Article

XXXX, Vol. XXX 000–000

Controlled Formation and Dynamic Wulff Simulation of Equilibrium Crystal Shapes of GaAs Pyramidal Structures on Nanopatterned Substrates

Ping-Show Wong,*,† Baolai Liang,† Ryan Molecke,‡ Jun Tatebayashi,† and Diana L. Huffaker†

†*Electrical Engineering Department, University of California at Los Angeles, Los Angeles, California 90095, and* ‡*Center for High Technology Materials, University of New Mexico, Albuquerque, New Mexico 87106*

Received July 9, 2009; Revised Manuscript Received March 1, 2010

ABSTRACT: The formation of GaAs pyramidal structures on nanopatterned GaAs substrates and the evolution of associated equilibrium crystal shapes (ECS) are systematically studied and simulated. Three distinct types of ECS are observed with high-resolution scanning electron microscopy (HRSEM), and they are defined by three crystal plane families including {11n}, {10n}, and (001). The controlled formation of these GaAs ECS is achieved through their growths in patterns of different opening diameters and under growth conditions of varying growth times and growth rates. Simulation results of the dynamic ECS model based on Wulff's theory not only strongly resemble the GaAs pyramidal structures in the HRSEM images but also successfully demonstrate the evolution progress of the ECS formation.

1. Introduction

Selective area growth of quantum dots (QDs) on nanopatterned substrates have recently drawn much scientific attention due to the extensive application potential in nanoscale electronic, optoelectronic, and photonic devices.[1−7] These applications result from the controlled size, dimension, and lithographic integration of the patterned QDs (PQDs). On masked GaAs (001) substrates with nanopatterned openings, the GaAs buffer layer for selective PQD nucleation are quantum structures in pyramidal forms. In the formation of these pyramidal structures under a certain set of growth conditions, an equilibrium crystal shape (ECS) will be assumed, which is determined by minimum surface free energy and thermodynamic equilibrium stability by atomic reconstruction and faceting in the microscopic scale.[8,9] Equilibrium crystal growth is actually rare except in very small particles and is hard to achieve experimentally because the surface transport of matters must be artificially facilitated for the lowest-energy atomic surface orientations to be reached.[10] However, the high-temperature growth conditions and small crystal size of semiconductors facilitate the equilibrated crystal formation,[11] which is aided by the fact that semiconductors are known to aggressively trade energy gained in bond formation with energy lost in elastic distortion in search of the lowest free energy geometrical configuration.[12]

The ECS, and the corresponding faceting and limiting crystal planes of these GaAs nanostructures, are crucial to the subsequent PQD nucleation to control the PQD size, shape, density, and optical properties.[3,13] In this work, we systematically study the formation of these GaAs ECS structures on nanopatterned substrates with different opening sizes and under various growth conditions including different growth times and growth rates. The observation and identification of the ECS faceting are achieved by means of high-resolution scanning electron microscopy (HRSEM). A dynamic model based on Wulff's theory[14] is also established to simulate the evolution of these GaAs ECS.

*To whom correspondence should be addressed.

2. Experimental Results and Discussion

Sample growth is carried out using a low-pressure (60 Torr) vertical Thomas-Swan metal−organic chemical vapor deposition (MOCVD) reactor with trimethyl-gallium and tertiarybutyl-arsine. The samples are grown on (001) GaAs substrates covered with a 25 nm thick SiO_2 mask. Circular features of 185, 225, or 275 nm in a diameter on a 330 nm pitch are opened in the mask surface to expose the GaAs substrate using interferometric lithography and dry etching.[15] The diameter of circular openings typically varies by ±10 nm. In the process, quarters of 2" wafers are patterned, and then cleaved into small pieces for epitaxial experiments. The growth temperature is 700 °C for all ECS sample growths.

While the formation of epitaxial GaAs pyramidal ECS varies with different pattern diameters and growth conditions, which will be shown later in the following paragraphs, variations of the GaAs ECS are also observed across a single sample, from the center to the edge, in a radial fashion. These variations are attributed to the higher effective adatom density at the edge region of the sample surface than at the center due to both gas phase diffusion and surface migration of the growth species at the wafer edge.[16] The vertical MOCVD reactor delivers uniform parallel flows of growth species from the showerhead to the rotating crucible (sample stage) and the sample. Because of the uniform temperature profile across the crucible, the growth species decompose into adatoms not only on top of the sample but also on other exposed part of the crucible. While adatoms generated atop the sample can readily be adsorbed onto pattern openings, others usually desorb from the exposed crucible surface. An adatom lateral concentration gradient is thus introduced, and these adatoms can move toward the sample in the following two mechanisms: the gas phase diffusion and the short-range adatom movement through atomic surface migration. Because of the continuous adatom adsorption onto the edge region of the sample surface and the limited adatom diffusion length, fewer adatoms are able to reach the center part of the sample. This results in an enhancement in the effective adatom density, and thus an increase in the growth rate, at the edge region of the sample surface. To facilitate the analysis of ECS variation across a single sample, in this study the patterned substrates are cleaved into 1 × 1 cm pieces for all epitaxial experiments, and three concentric regions are subsequently defined across the typical sample: the center region, the middle region, and the edge region. All following ECS studies with different ECS growth pattern diameters and growth conditions will compare and analyze the ECS variation in these three regions to better understand their roles and effects on the ECS formation.

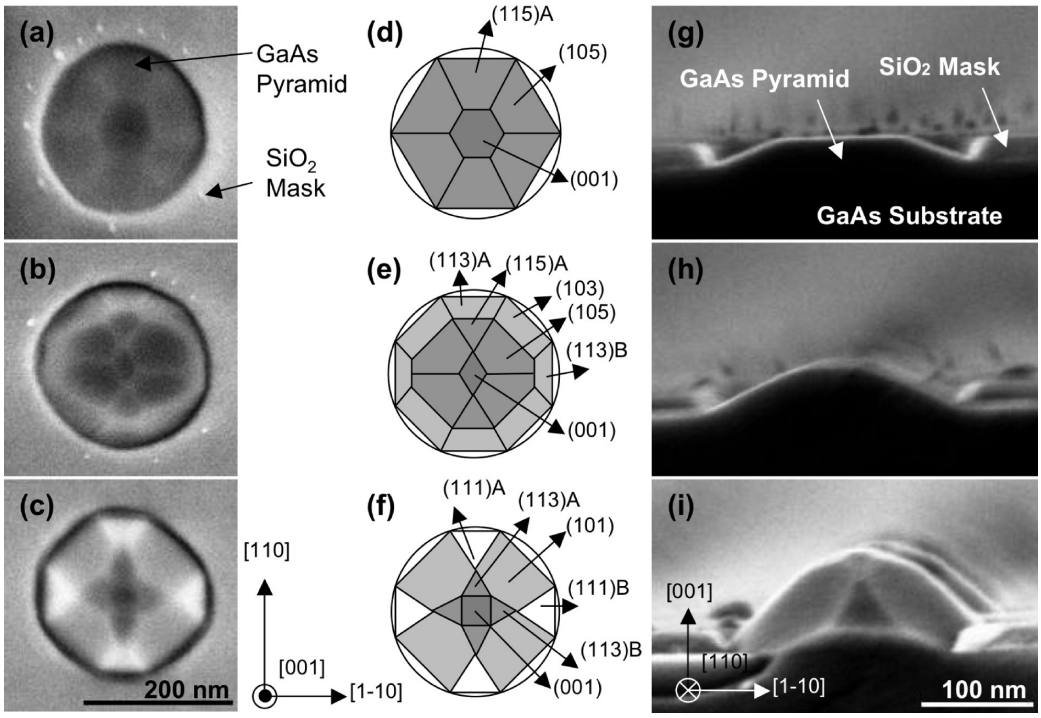

Figure 1. (a−c) The plan-view SEM images, (d−f) the schematics, and (g−i) the cross-sectional SEM images of the three unique types of GaAs ECS pyramidal structures.

Among all pyramidal shapes observed across samples with different pattern sizes and growth conditions, only three distinct types of ECS are identified, which was previously reported by the authors and summarized below.[3] Figure 1a−c shows the plan-view HRSEM images of the GaAs ECS structures formed on samples with patterns of 225 nm in diameter, while Figure 1d−f shows schematic illustrations of the limiting crystal facets of these structures. Pyramid A in Figure 1a has six hexagonal facets representing {115} and {105} groups, and a (001) apex. Pyramid B in Figure 1b is defined by the {115}, {105}, steeper {113} and {103} facet groups, and a (001) apex. Pyramid C in Figure 1c is defined by {113}, the steepest {111} and {011} facet groups with a (001) apex. The HRSEM images of the corresponding cross-sectional profiles of these GaAs pyramids are shown in Figure 1g−i to elucidate the pyramid geometry. The images indicate a pyramidal height ranging from ~30 to 90 nm for the three types of ECS. It is important to note two special characteristics of the ECS formation described in this work. First, there are boundary conditions imposed by the SiO_2 mask and the GaAs substrate. Second, the formation of these ECS is an evolution process due to the nature of the epitaxial growth, and as shown in later paragraphs, Pyramid C is considered the final stage of the evolution and evolves from Pyramid B, which evolves from Pyramid A.

While the formation of ECS results from the minimization of the total surface energy of the nanostructure, the surface energy of a certain crystal plane changes with different surface atomic structures and the presence of adjacent facets. Moll et al. and Platen et al. carried out the calculation of surface energy using density-functional theory,[8,17] where the surface energies of GaAs crystal planes of various orientations, surface reconstructions, and neighboring facets are functions of the difference between the chemical potentials of arsenic and arsenic bulk. The chemical potential and surface reconstruction of a crystal plane are determined by growth conditions including the growth temperature and the arsenic overpressure, which means ECS formed under different growth conditions may develop different facets to minimize the total surface energy. This can explain the observation of other high-indexed {11n} and {1 nm} facets by other studies in different experimental environments.[1,18−21] The anisotropic formation of (115)A facets on Pyramid A, compared to the almost isotropic formation of {111} and {113} planes, may also come from the different termination of (11n)A and B type surfaces.[22−24]

ECS Control by Pattern Diameter. Figure 2 shows the SEM images and corresponding statistics of the GaAs ECS volume formed on patterns with different pattern diameters. These samples are grown under the same growth conditions: planar growth rate of 1 Å/s, growth time of 15 s, and the V−III ratio at 12.5. Both the plan-view and cross-sectional SEM images are used to measure dimensions of the pyramidal structures to calculate their volumes. Figure 2a−c are the SEM images taken from the center, middle, and edge region of the sample with a pattern diameter of 275 nm, respectively. These SEM images were taken within roughly the 10-μm-by-10-μm regions around the corresponding exact sampling points at 0 (center region), 2.5 (middle region), and 5 mm (edge region) from the center of the 1-cm-by-1-cm substrates in order to obtain the clearest and most representative images. In the same fashion, Figure 2, panels d−f are images from the three regions of the sample with a pattern diameter of 225 nm, and Figure 2g−i from the sample with a pattern diameter of 185 nm. The SEM images clearly indicate that the shape, and volume, of the GaAs ECS varies from the center region of the sample to the edge region.

From the statistics of the calculated volume of these pyramidal ECS structures, there is little material deposition in the center region of the 275-nm sample, but the volume of the ECS increases rapidly from the center region toward the edge region of the sample. For the 225-nm sample, there is a higher amount of material deposited in the center region, compared to the 275-nm sample, but the increase in ECS volume from the center to the edge is slower. In the case of the 185-nm sample, with the largest ECS volume in the center, there is almost no change of ECS volume from the center to the edge. It should be noted that the amount of growth species delivered to the sample surface is the same for these samples with different pattern diameters and filling factors. The 185-nm sample has the smallest filling factor, and the least amount of materials is required to formed Pyramid C, the last stage of the ECS evolution process, in the edge region. Excess materials are hence available for the middle and center regions through diffusion. In contrast, the 275-nm sample has the largest filling factor and consumes more materials to form completed Pyramid C. Hence, fewer adatoms are available through diffusion for the middle and center regions.

ECS Control by Growth Time. For the growth time experiment, growth periods of 1, 2, 4, and 8 s are used, while the GaAs planar

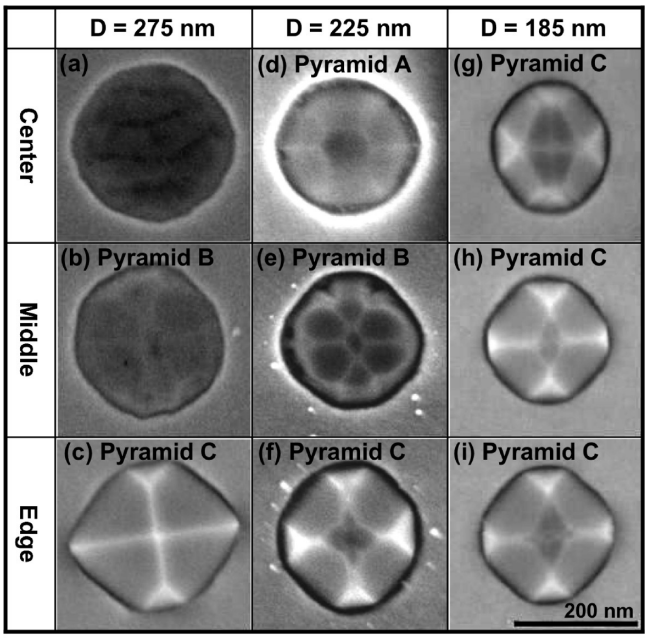

Figure 2. SEM images and volume statistics of the ECS structures formed in patterns of different diameters. Labels of the data points correspond to labels of the SEM images.

growth rate is kept at 0.5 Å/s, and the V−III ratio at 12.5. Figure 3 shows the SEM images of a series of samples with varying growth time. Figure 3a−c are from the center, middle, and edge region of the sample with a growth time of 1 s, respectively. Figure 3d−f is from the 2-s sample, Figure 3g−i is from the 4-s sample, and Figure 3j−l is from the 8-s sample. With the growth time of 1 s, there is almost no pyramidal structure formed in the center and middle region of the sample, while the ECS in the edge region assumes the form of Pyramid A. With the growth time of 2 s, ECS of Pyramid A starts to appear in the middle region, and ECS in the edge region becomes Pyramid C. When the growth time is further increased to 4 s, ECS of Pyramid A begins to appear in the center region as well, and Pyramid A in the middle region becomes Pyramid B, while the Pyramid C in the edge region retains the same form but with increased volume. With the longest growth time of 8 s, the shape of the GaAs pyramids stays almost the same and the volume seems to saturate in all three regions. These pyramidal structures evolve with the increasing growth time, and the volume saturates under a certain ECS. The saturation condition is met when the adatom adsorption and desorption reach equilibrium and the self-size-limiting effect of the facets takes place. These saturation ECS, that is, the limiting facets, may be different under different growth conditions and in different regions. Pyramid C is considered the final form of ECS under this growth mode and evolves from Pyramid B, which evolves from Pyramid A. The increase in ECS volume before the saturation is not linearly proportional to the increase in growth time because different facets of different surface areas and surface dynamics are available for adatom adsorption at different stages of the ECS evolution. It can also be clearly observed that the three types of GaAs ECS can be formed practically anywhere on the sample in a controllable fashion.

ECS Control by Growth Rate. The (planar) growth rate, that is, the rate at which the growth species are delivered to the sample surface, can also be used to control the formation of ECS. Experiments with different planar growth rates of 0.125 Å/s (for 16 s), 0.5 Å/s (for 4 s), and 2 Å/s (for 1 s), all with a V−III ratio of 12.5, are carried out. The total amount of material delivered to the sample surface is held constant for all three samples. Figure 4a−c is from the center, middle, and edge region of the sample with a growth rate of 0.125 Å/s, Figure 4d−f is from the 0.5 Å/s sample, and Figure 4g−i is from the 2 Å/s sample. The ECS volume is observed to decrease with increasing growth rates, which may be explained as that the adsorption of the adatoms onto the existing GaAs structures is a process near the reaction-limiting regime for the range of parameters explored here. The samples with slower adatom flow rates have longer growth times, and hence more time for adatom adsorption to form larger ECS.

3. Simulation Results and Discussion

As suggested in previous paragraphs, the formation of GaAs ECS on nanopatterned substrates can be controlled by various growth and pattern parameters. At the same time, the ECS faceting is generally driven by the minimization of surface free energy and stabilization of thermodynamic equilibrium stability. To understand the formation and evolution of GaAs ECS pyramids and the associated faceting under boundary conditions, Wulff's theory is employed to simulate the dynamic progression. Wulff's classical theory relates the polar plot of a given material's anisotropic surface energies to the expected ECS, which is the shape with the lowest surface energy for a given volume. As depicted in Figure 5, the Wulff shape is the convex envelop bound by all hyperplanes normal to the radial vectors emanating from the origin to the surface energy function. The surface energy at angle θ, $\gamma(\theta)$, is related to the expected Wulff crystal shape by the following equation:[25]

$$W = \{x \in R^d : x \cdot \theta \leq \gamma(\theta), \text{ for all } \theta \in S^{d-1}\}$$

where S^{d-1} refers to a surface in polar or spherical coordinates, R^d is the real domain of d dimensions ($d = 2$ or 3) containing all vectors x. The orientation of the ECS limiting facets has been shown to be a reliable source of related information on surface energy when observed crystal shapes are fitted to theoretical expression. It has been demonstrated in experiments by Bonzel and Surnev that the anisotropic surface energy and step energy are correlated in Pb particles on Cu (111).[26]

The modeling of the Wulff shape formation is carried out by using Matlab[27] programming with 3D visualization tools. The program generates 3D multifaceted objects based on the Wulff theory, and the choice of available facet planes and their corresponding surface energies are adjusted accordingly for fitting after being visually compared to the experimentally observed Pyramids A, B, and C. The best-fitted simulation results are shown in Figure 6. The simulated Wulff pyramids, Figure 6a−c in bird-eye view and plan-view, strongly resemble the GaAs ECS in the SEM images, Figure 1a−c. The small discrepancies in the shape and size of the facets near the edge of circular openings might come from the deviation of the GaAs

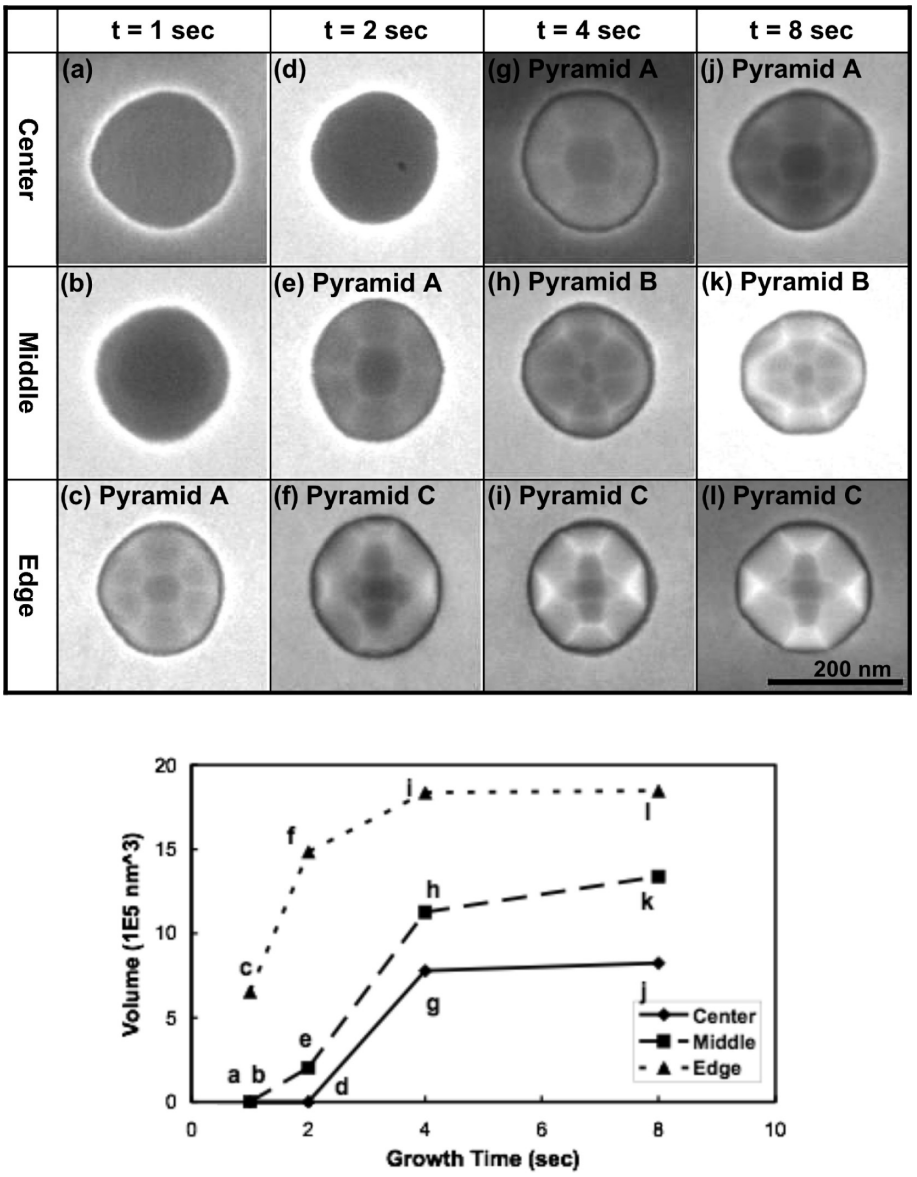

Figure 3. SEM images and volume statistics of the ECS structures formed with different growth times. Labels of the data points correspond to labels of SEM images.

pyramids from the optimal equilibrium crystal epitaxial growth conditions due to the existence of boundary conditions, including the SiO_2 mask and the GaAs substrate. On the basis of the information of facets' relative surface energies compared to the reference (001) top facet for Pyramids A, B, and C, this model is constructed to dynamically simulate the time-evolving ECS, where the evolution of surface energies is linked to the evolution of the ECS. As the simulation results show, the relative surface energies of {10n} and {11n} planes increase gradually in the emerges of the lower-indexed {111} and {101} planes, while {103} facets regress, when the ECS evolves from Pyramid B to Pyramid C. On the other hand, as previously discussed the surface energies of ECS facet, including the (001) plane, may change when formed under different growth environments or with different neighboring facets. This indicates the relative anisotropic surface energy function can be different for various stages of the ECS evolution, which also suggests that the surface bonding and the atomic surface dynamics of a certain nanofacet may change in the continuous epitaxial process. The Wulff's theory thus provides a powerful tool to study the GaAs ECS facet surface energy hierarchy and the surface dynamics.

In conclusion, we have demonstrated the controlled formation of GaAs ECS on nanopatterned GaAs substrates. GaAs ECS pyramids are shown to form with different limiting crystal facets under different pattern diameters and growth conditions, including the growth time and the growth rate. The ECS growth variation from the center to the edge region of the sample due to adatom diffusion is observed and statistically explained. Across different regions of all samples under varying growth environments, three distinct types of GaAs ECS are identified, and they are defined by crystal plane families including {11n}, {10n}, and (001). It is also shown that these three pyramids can be formed anywhere on the sample in a controllable fashion by adjusting growth parameters. The simulation results based on Wulff's theory show close similarity with the observed ECS and successfully

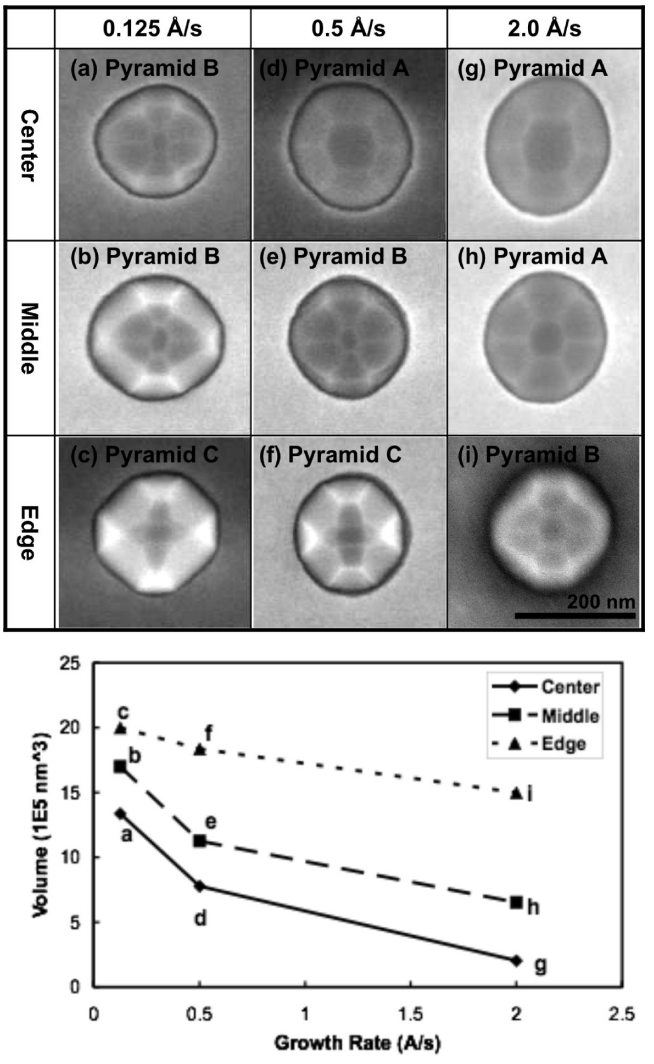

Figure 4. SEM images and volume statistics of the ECS structures formed under different growth rates. Labels of the data points correspond to labels of the SEM images.

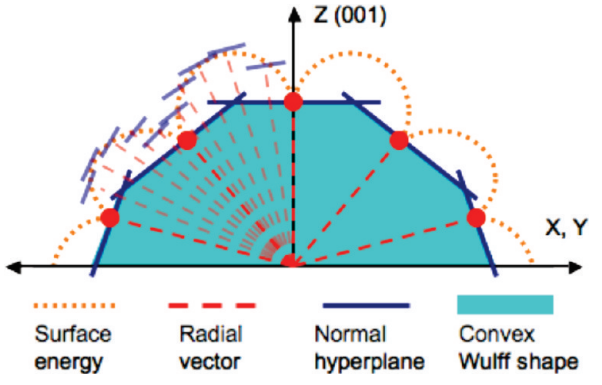

Figure 5. The construction of Wulff shape based on the anisotropic surface energy.

demonstrate the dynamic evolution of these GaAs ECS. These experimental data and theoretical simulation results have thus laid the fundamental groundwork in understanding the formation mechanism of GaAs pyramidal ECS and the subsequent controlled nucleation of QDs on nanopatterned substrates.

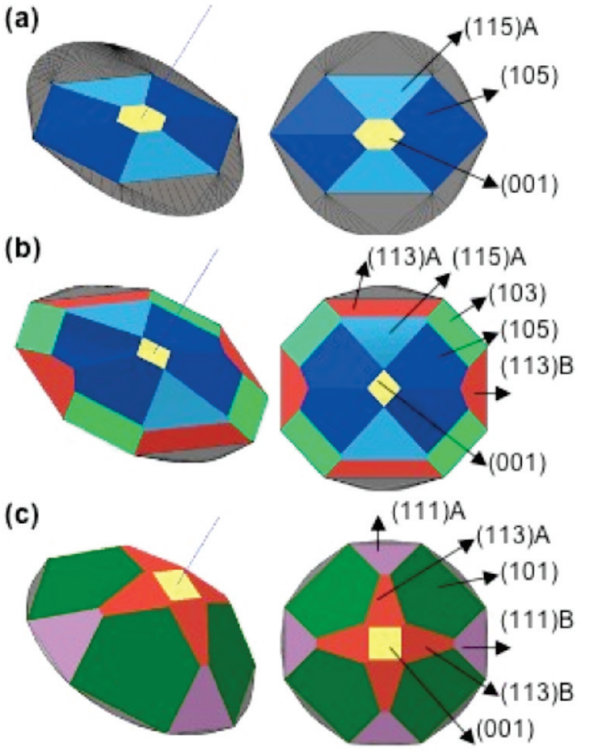

Figure 6. (a−c) Simulation results of Wulff-fit pyramid shapes.

Acknowledgment. The authors acknowledge the financial support of the NSF through Grant ECCS-0824273.

References

(1) Umeda, T.; Kumakura, K.; Motohisa, J.; Fukui, T. *Physica E* **1998**, *2*, 714–719.
(2) An, H.; Motohisa, J. *Appl. Phys. Lett.* **2000**, *77*, 385–387.
(3) Wong, P. S.; Balakrishnan, G.; Nuntawong, N.; Tatebayashi, J.; Huffaker, D. L. *Appl. Phys. Lett.* **2007**, *90*, 183103.
(4) Wong, P. S.; Liang, B. L.; Tatebayashi, J.; Xue, L.; Nuntawong, N.; Kutty, M. N.; Brueck, S. R. J.; Huffaker, D. L. *Nanotechnol.* **2009**, *20*, 035302.
(5) Chithrani, D.; Williams, R. L.; Lefebvre, J.; Poole, P. J.; Aers, G. C. *Appl. Phys. Lett.* **2004**, *84*, 978–980.
(6) Hsieh, T. P.; Chyi, J. I.; Chang, H. S.; Chen, W. Y.; Hsu, T. M.; Chang, W. H. *Appl. Phys. Lett.* **2007**, *90*, 073105.
(7) Lee, J. H.; Wang, Zh. M.; Liang, B. L.; Black, W. T.; Kunets, Vas P.; Mazur, Yu I.; Salamo, G. J. *Nanotechnology* **2006**, *17*, 2275–2278.
(8) Moll, N.; Kley, A.; Pehlke, E.; Scheffler, M. *Phys. Rev. B* **1996**, *54*, 8844–8855.
(9) Lee, S. C.; Brueck, S. R. J. *J. Appl. Phys.* **2004**, *96*, 1214–1218.
(10) Dobrushin, R. L.; Kotecky, R.; Shlosman, S. B. *J. Stat. Phys.* **1993**, *72*, 1–14.
(11) Gadewar, S. B.; Hofmann, H. M.; Doherty, M. F. *Cryst. Growth Des.* **2004**, *4*, 109–112.
(12) Zangwill, A. *Physics at Surfaces*; Cambridge University Press: New York, 1988; pp 205−222.
(13) Liang, B. L.; Wong, P. S.; Nuntawong, N.; Albrecht, A. R.; Tatebayashi, J.; Rotter, T. J.; Balakrishnan, G.; Huffaker, D. L. *Appl. Phys. Lett.* **2007**, *91*, 243106.
(14) Dobrushin, R. L.; Kotecky, R.; Shlosman, S. *Wulff Construction: A Global Shape from Local Interaction*; American Mathematical Society: Providence, RI, 1993.
(15) Lee, S. C.; Malloy, K. J.; Breuck, S. R. J. *J. Appl. Phys.* **2001**, *90*, 4163–4168.
(16) Sasaki, T.; Kitamura, M.; Mito, I. *J. Cryst. Growth* **1993**, *132*, 435–443.
(17) Platen, J.; Kley, A.; Setzer, C.; Jacobi, K.; Ruggerone, P.; Scheffler, M. *J. Appl. Phys.* **1999**, *85*, 3597–3601.

(18) Nishiwaki, T.; Yamaguchi, M.; Sawaki, N. *Jpn. J. Appl. Phys.* **2009**, *48*, 071102.
(19) Araki, M.; Hanada, Y.; Fujikura, H.; Hasegawa, H. *Jpn. J. Appl. Phys.* **1997**, *36*, 1763–1769.
(20) Ramdani, R. M.; Gil, E.; Andre, Y.; Trassoudaine, A.; Castelluci, D.; Paget, D.; Rowe, A. C. H.; Gerard, B. *J. Cryst. Growth* **2007**, *306*, 111–116.
(21) Yazdanpanah, V. R.; Wang, Z. M.; Salamo, G. J. *Appl. Phys. Lett.* **2003**, *82*, 1766–1768.
(22) Young, K.; Kahn, A. *J. Vac. Sci Technol. A* **1987**, *5*, 654–655.
(23) Wang, Z. M.; Daweritz, L.; Ploog, K. H. *Appl. Phys. Lett.* **2001**, *78*, 712–714.
(24) Wang, Z. M.; Yazdanpanah, V. R.; Shultz, J. L.; Salamo, G. J. *Appl. Phys. Lett.* **2002**, *81*, 2965–2967.
(25) Peng, D. P.; Osher, S.; Merriman, B.; Zhao, H. K. *Contemp. Math.* **1999**, *238*, 251–303.
(26) Bonzel, H. P. Surnev, S. *Dynamics of Crystal Surfaces and Interfaces*; Plenum Press: New York; 1997; pp 41− 52.
(27) Product of The Mathworks, Inc. (http://www.mathworks.com/). The Matlab software used is student version 7.1.0.124.